Supplementary Material

1 SUPPLEMENTARY METHOD

1.1 Non-equilibrium molecular dynamics (NEMD) method

Planar shock wave is produced by slamming the sample upon against a piston. A shock wave propagates into a single crystal Cu target, achieving a supported high pressure and high temperature shock state. Three directions are explored: (010) for x-axis, (001) for y-axis and (100) for z-axis. Periodic boundaries are applied along the x- and y-axes, and a fixed boundary is adopted along the z-axis. Different system sizes have been used to check the convergence of simulations, as shown in Table. S1. The results from these system sizes are consistent with previous works. System sizes of 2160000 atoms is used in NEMD simulations (Fig. S1). The trajectories of atoms under different pressure (32, 75, 88, 98, 180 GPa) corresponding to different piston velocity (0.76, 1.43, 1.6, 1.73, 2.65 km/s) have been shown in MP4 files.

1.2 Multi-Scale Shock Technique (MSST) method

The method simulates the propagation of shock waves using the Euler equations for compressible flow. Based on the conservation of mass, momentum, and energy, respectively, everywhere in the wave. It is a tractable method that operates constant shock velocity by time-evolving equations of motion for the atoms and volume of the computational cell to constrain the shock propagation direction stress to the Rayleigh line and energy to the Hugoniot energy condition. For a specified shock speed, the Hugoniot relations describe a steady planar shock wave within continuum theory. The Hugoniot relations can be determined as,

$$u=v_s(1-\frac{\rho_0}{\rho}),$$
$$p-p_0=v_s{}^2\rho_0(1-\frac{\rho_0}{\rho}),$$
$$e-e_0=p_0(\frac{1}{\rho_0}-\frac{1}{\rho})+\frac{v_s^2}{2}(1-\frac{\rho_0}{\rho})^2.$$

Here u is particle velocity, v_s is shock speed, ρ is the density, e is the energy per unit mass, and p is pressure in the direction of shock propagation. The molecular dynamics simulation utilize a well-established extended Lagrangian approach,

$$L=T(\{\dot{\vec{r}}_i\})-V(\{\vec{r}_i\})+\frac{1}{2}Q\dot{v}^2+\frac{1}{2}\frac{v_s^2}{v_0^2}(v_0-v)^2+p_0(v_0-v),$$

where T and V are kinetic and potential energies per unit mass, Q is a masslike parameter for simulation cell size, and v is the specific volume. The equation of motion for the system volume is

$$Q\ddot{v}=\frac{\partial T}{\partial v}-\frac{\partial V}{\partial v}-p_0-\frac{v_s^2}{v_0^2}(v_0-v).$$

The detailed description of MSST method can be discussed in ref(Reed et al., 2003) by Reed *et al.*

1.3 Adaptive Common neighbor analysis (a-CNA) method

In this technique, the local structures are analyzed by the environment of the pairs. A characteristic signature is captured from the topology of bonds that connect the surrounding neighbor atoms. A sequence of three criteria specifies the pairs of atoms. The first criterion is the number of near-neighbors shared by the root pair of atoms. The second criterion is the number of bonds between these common neighbours. The third criterion is the number of bonds in the longest continuous chain. These three characters are sufficient to characterize the classification of pairs of atoms with a specified cutoff distance of each other. Different types of pairs are associated with different types of local order, in particular FCC, HCP, BCC, and

OTHER. The right cutoff radius is hard to be found, but the a-CNA determines the optimal cutoff radius automatically (detailed in ref(Tsuzuki et al., 2007; Stukowski, 2012)).

1.4 Effective coordination number (ECN) method

The standard coordination number (CN) takes into account that a particular atom is surrounded by atoms at different distances, while the CN attributes a unique weight for all bonds independently of bond lengths. Thus, the values obtained for the CN depend on the cutoff bond length. The ECN concept can be independent of the choice of the bond cutoff, and therefore provides a more accurate method to determine possible structural trends with different bond lengths in disordered structures. The ECN and bond length for all atoms in the cluster can be obtained by an exponential averaging function. The ECN_i is obtained by the following set of equations:

$\mathrm{ECN}_i=\Sigma_j exp[1-(\frac{d_{ij}}{d_{av}^i})^6]$,

where d_{ij} is the distance between atom i and j, while d_{av}^i is defined as

$$d_{av}^i=\frac{\Sigma_j d_{ij} exp[1-(\frac{d_{ij}}{d_{av}^i})^6]}{\Sigma_j exp[1-(\frac{d_{ij}}{d_{av}^i})^6]}$$

in which d_{av}^i is obtained self-consistently, i.e., $|d_{av}^i(new) - d_{av}^i(old) < 0.0001|$. The average ECN and d_{av} for a particular configuration are obtained by

$\mathrm{ECN}=\frac{1}{N}\Sigma_{i=1}^N \mathrm{ECN}_i$

and

$d_{av}=\frac{1}{N}\Sigma_{i=1}^N d_{av}^i$, where N is the total number of atoms in the cluster (detailed in ref(Piotrowski et al., 2010)).

1.5 Free energy calculations

Standard equilibrium free energy calculations are often performed by the construction of a series of equilibrium states on a path between two thermodynamic states of interest. In addition, every state requires a separate simulation for sufficient equilibration. The free energy difference ($\triangle$F) between two states of interest is obtained by computing ensemble averages of a set of the relevant these states, followed by numerical integration. The method related $\triangle F$ to the reversible work W_{rev} along a quasistatic path. For a system of N particles in NVT ensemble, the Hamiltonian is given by H(Γ, λ), Γ is a point in the phase space and λ is a parameter. The canonical partition function of system is:

$Z(N,V,T;\lambda)=\int \frac{d\Gamma}{h^{3N}} exp[-\beta \mathrm{H}(\Gamma,\lambda)]$,

the Helmholtz free energy of this system is:

$F(N,V,T;\lambda)=-k_B \mathrm{T} \ln Z(N,V,T;\lambda)$,

where $\beta=\frac{1}{k_B \mathrm{T}}$, k_B is the Boltzmann constant and h is Planck's constant. Consider two thermodynamic states characterized by different λ from 0 to 1, the parametrical Hamiltonian H(λ) is given by

$\mathrm{H}(\lambda)=\lambda \mathrm{H}_f+(1-\lambda)\mathrm{H}_i$,

where H_i and H_f represent two different Hamiltonians. The desired free energy difference can be obtained by the derivative of the Helmholtz free energy with respect to λ,

$\frac{\partial F}{\partial \lambda}=\frac{1}{\mathrm{Z}}\int \frac{d\Gamma}{h^{3N}} \frac{\partial \mathrm{H}}{\partial \lambda} exp[-\beta \mathrm{H}(\Gamma,\lambda)]=\left\langle \frac{\partial \mathrm{H}}{\partial \lambda} \right\rangle_\lambda$,

where $\langle ... \rangle_\lambda$ is canonical ensemble average for a particular value of λ, the free energy difference is equal to the intergration of this differential equation,

$\triangle F$=$F(\lambda_f)$-$F(\lambda_i)$=$\int_{\lambda_i}^{\lambda_f} \mathrm{d}\lambda \langle \frac{\partial \mathrm{H}}{\partial \lambda} \rangle_\lambda \equiv W_{i\to f}^{rev}$,
Where i and f are states of interest and reference, respectively. In the equilibrium thermodynamic integration (TI) method, the integration is equal to reversible work along a quasistatic path between two equilibrium states of interest. In contrast to a quasistatic process, the work done along a nonequilibrium process is the irreversible work, and the dissipated heat is generated along the path. The nonequilibrium approaches, related $\triangle F$ to the irreversible work by connecting its mean value to the reversible work, are performed sufficiently closed to ideally quasistatic process between two equilibrium states of interest. The average dissipated heat for two processes between *i* and f states are the same (*i.e.* $\overline{E_{i\to f}^{diss}}$=$\overline{E_{f\to i}^{diss}}$). So, the expression is given by

$\triangle F$=W_{rev}=$\overline{W_{irr}}$-$\overline{E_{diss}}$=$\frac{1}{2}$[($\overline{W_{i\to f}^{irr}}$-$\overline{E_{i\to f}^{diss}}$)-($\overline{W_{f\to i}^{irr}}$-$\overline{E_{f\to i}^{diss}}$)]=$\frac{1}{2}$($\overline{W_{i\to f}^{irr}}$-$\overline{W_{f\to i}^{irr}}$).

The nonequilibrium approach estimates the path in terms of an explicitly time dependent process with the function of λ=λ(t), the irreversible work between two states (λ_i(t=0)=0, λ_f(t=t_s)=1) is given by

$W_{i\to f}^{irr}$=$\int_0^1 \mathrm{d}\lambda \langle \frac{\partial \mathrm{H}}{\partial \lambda} \rangle_\lambda$=$\int_0^{\mathrm{t_s}} dt \frac{d\lambda}{\mathrm{dt}} (\frac{\partial \mathrm{H}}{\partial \lambda})_{\Gamma(\mathrm{t})}$,
where t_s is a switching time. For computing the free energy of solid, the reference system of Einstein crystal $F_E(N,V,T)$ is chosen, detailed discussion can be found in ref(Freitas et al., 2016). In the canonical ensemble (NVT) the Helmholtz free energy F is given by the following expression:

$$F(N,V,T) = F_E(N,V,T) + \triangle F,$$
then, the Gibbs free energy G can be obtained as:

$$G = F(N,V,T) + PV.$$

The shock-induced BCC structures are generated by MSST simulations in the shock velocity of 6.4 and 7.4 km/s, corresponding to 97 GPa, 1600 K and 156 GPa, 3400 K. To avoid the occurrence of structural transformation, we restricted the free energy calculations of shock-induced BCC structure around the Hugoniot curves. The FCC and shock-induced BCC structures including 24000 atoms are relaxed in NPT ensembles for 100, 200, 300, 400 and 500 ps under the pressure of 120$\sim$175 GPa. Then the nonequilibrium thermodynamic integration (ne-TI) are kept for NVT ensembles in simulations. The system is set equilibrium for 100 ps before the switching starts, followed by a persisting 200 ps switching duration time. Synthesizing both simulations, we found no sign of phase transition under 6.4 km/s since the Gibbs free energy difference between FCC and shock-induced BCC phase is positive from 1000 K to 3000 K. While, for shock velocity under 7.4 km/s, as presented in Fig. S6, we found the phase transition is triggered. The fitting curves are obtained by second order polynomial functions(Straatsma and Berendsen, 1988; Taniuchi and Tsuchiya, 2018).

REFERENCES

Freitas, R., Asta, M., and De Koning, M. (2016). Nonequilibrium free-energy calculation of solids using lammps. *Computational Materials Science* 112, 333–341

Piotrowski, M. J., Piquini, P., and Da Silva, J. L. (2010). Density functional theory investigation of 3 d, 4 d, and 5 d 13-atom metal clusters. *Physical Review B* 81, 155446

Reed, E. J., Fried, L. E., and Joannopoulos, J. (2003). A method for tractable dynamical studies of single and double shock compression. *Physical review letters* 90, 235503

Straatsma, T. and Berendsen, H. (1988). Free energy of ionic hydration: Analysis of a thermodynamic integration technique to evaluate free energy differences by molecular dynamics simulations. *The Journal of chemical physics* 89, 5876–5886

Stukowski, A. (2012). Structure identification methods for atomistic simulations of crystalline materials. *Modelling and Simulation in Materials Science and Engineering* 20, 045021

Taniuchi, T. and Tsuchiya, T. (2018). The melting points of mgo up to 4 tpa predicted based on ab initio thermodynamic integration molecular dynamics. *Journal of Physics: Condensed Matter* 30, 114003

Tsuzuki, H., Branicio, P. S., and Rino, J. P. (2007). Structural characterization of deformed crystals by analysis of common atomic neighborhood. *Computer physics communications* 177, 518–523

2 SUPPLEMENTARY TABLES AND FIGURES

2.1 Tables

Table S1. Different size of the configurations for NEMD simulations along z-direction. u is piston velocity, ρ_0 is initial density, ρ is the density after the impact, and P is shock pressure.

No. of atoms	Size(nm)			Orientation			u(km/s)	ρ_0(g/cm^3)	ρ(g/cm^3)	P(GPa)
	x	y	z	x	y	z				
216×10^4	10.85	10.85	216.9	010	001	100	1.60	8.81	11.86	88.71
1944×10^4	32.54	32.54	216.9	010	001	100	1.60	8.81	11.87	88.57
5400×10^4	54.23	54.23	216.9	010	001	100	1.60	8.81	11.87	88.57

2.2 Figures

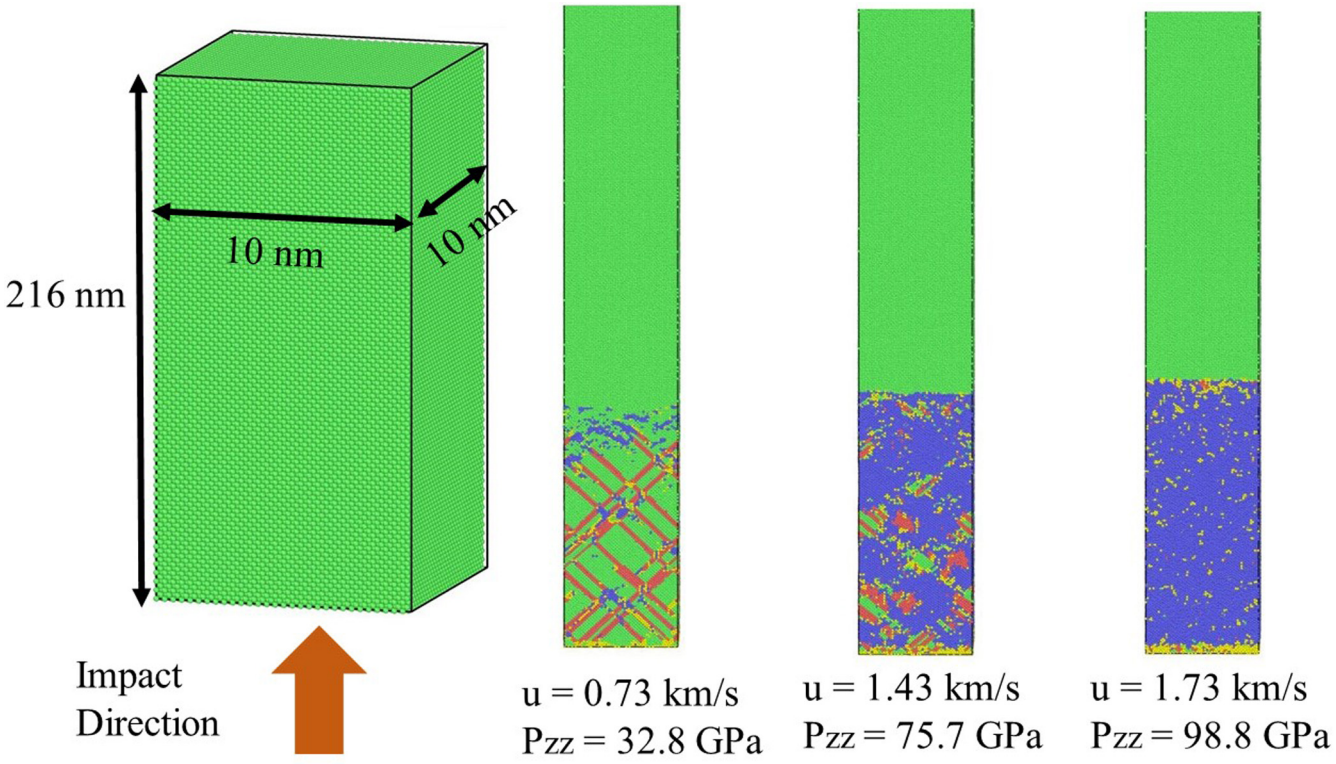

Figure S1. NEMD simulations of Cu under shock compression. The initial configuration of simulation (left panel) and the structures under different pressures (right panel).

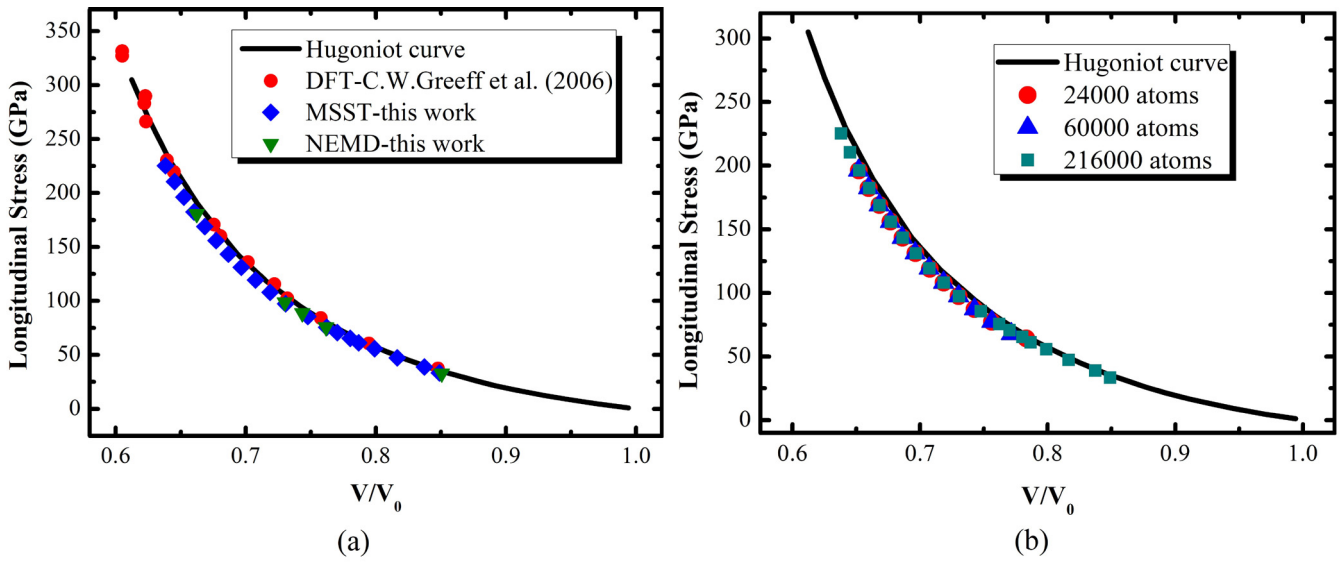

Figure S2. Longitudinal stress vs volume compressions for compressed copper. (a) The results of NEMD and MSST simulations based on EAM potential in comparison with previous Hugoniot curve and DFT results. Five typical piston velocities (0.763, 1.43, 1.6, 1.73, 2.65 km/s) have been simulated by NEMD approach. (b) Different configurations are compared for MSST simulations.

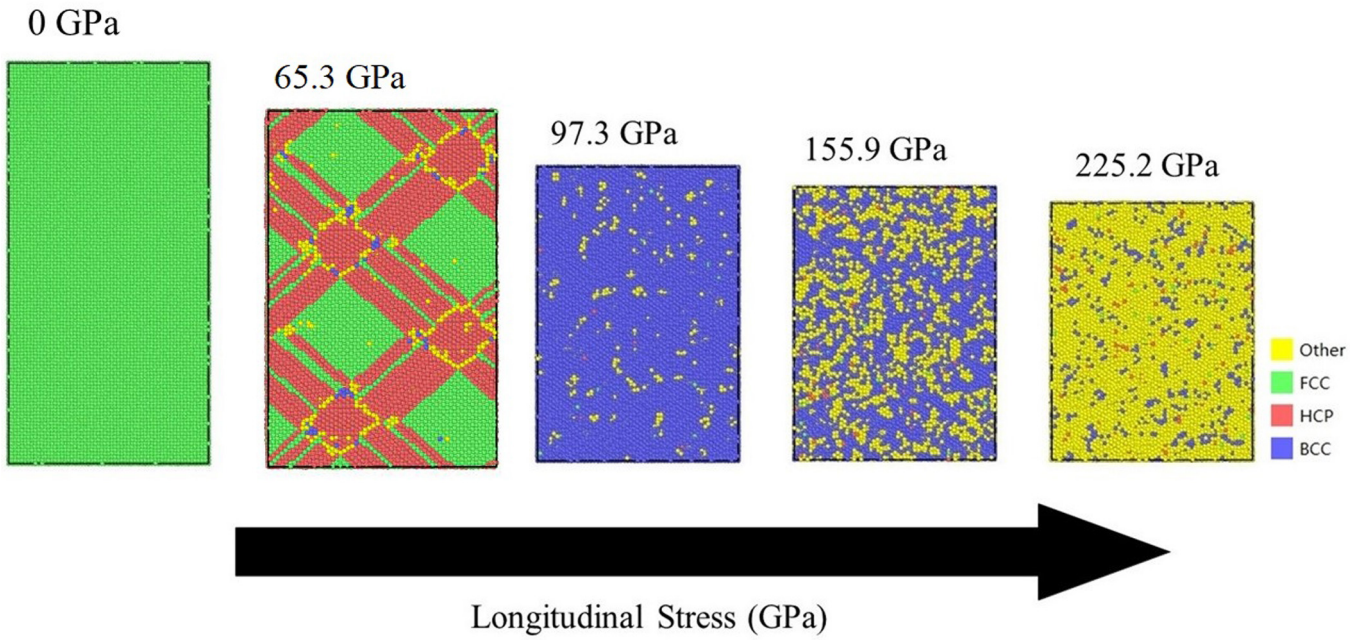

Figure S3. Structural transformation path of shock compression through MSST simulation are presented.

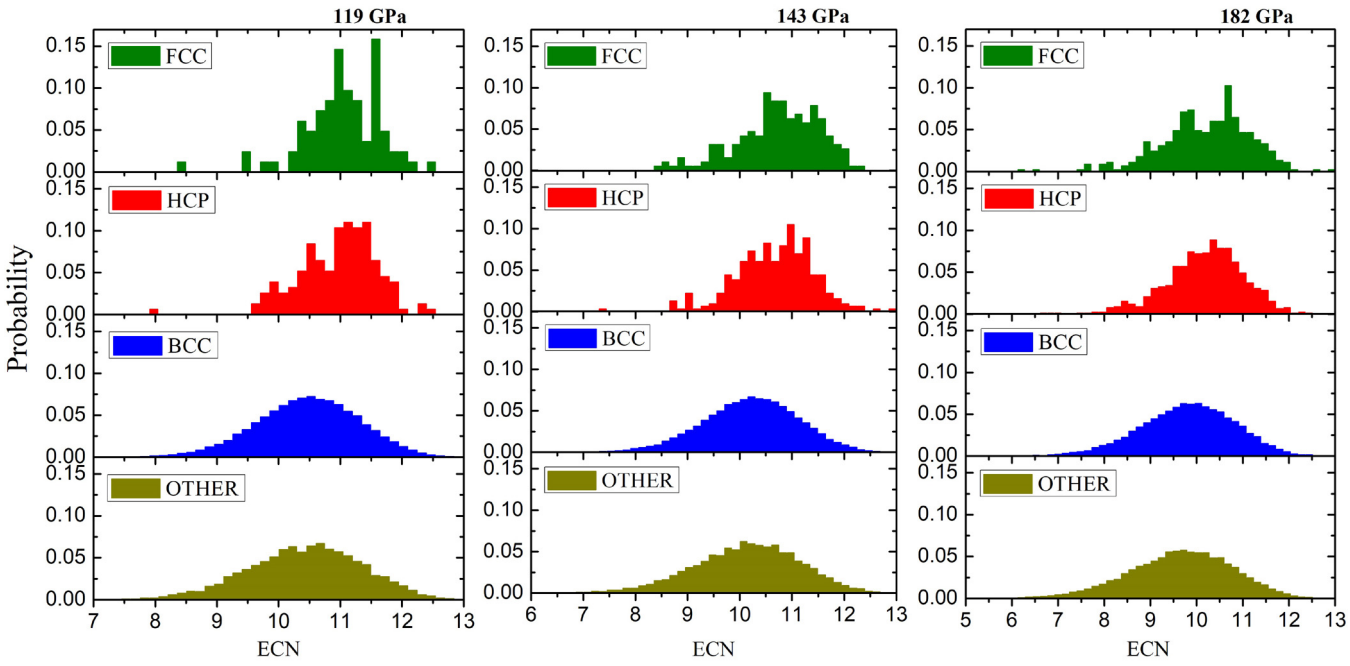

Figure S4. The ECN distribution of atoms with four structure types under different shock pressure.

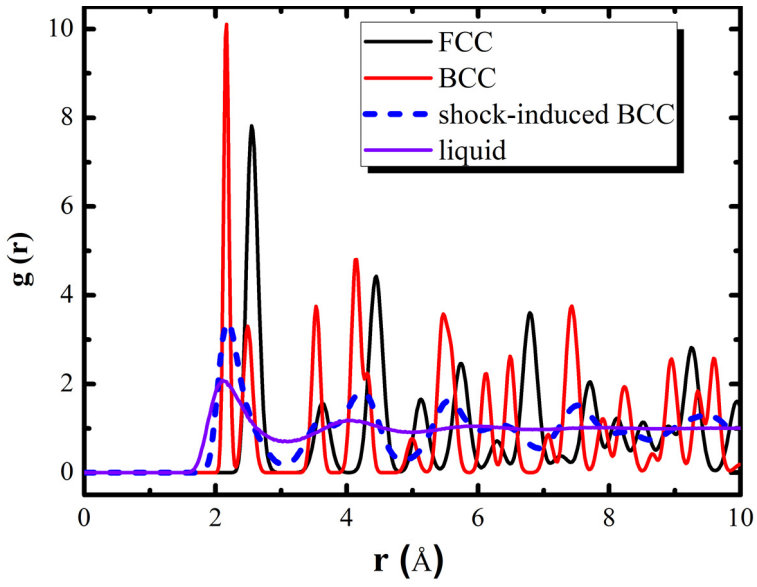

Figure S5. The RDF curves of different crystals. Black solid line denotes the RDF of initial FCC, red solid line denotes the RDF of perfect BCC under static pressure of 156 GPa, blue short dot denotes shock-induced BCC under shock pressure of 156 GPa, and purple solid line denotes the RDF of liquid copper under static pressure of 156 GPa.

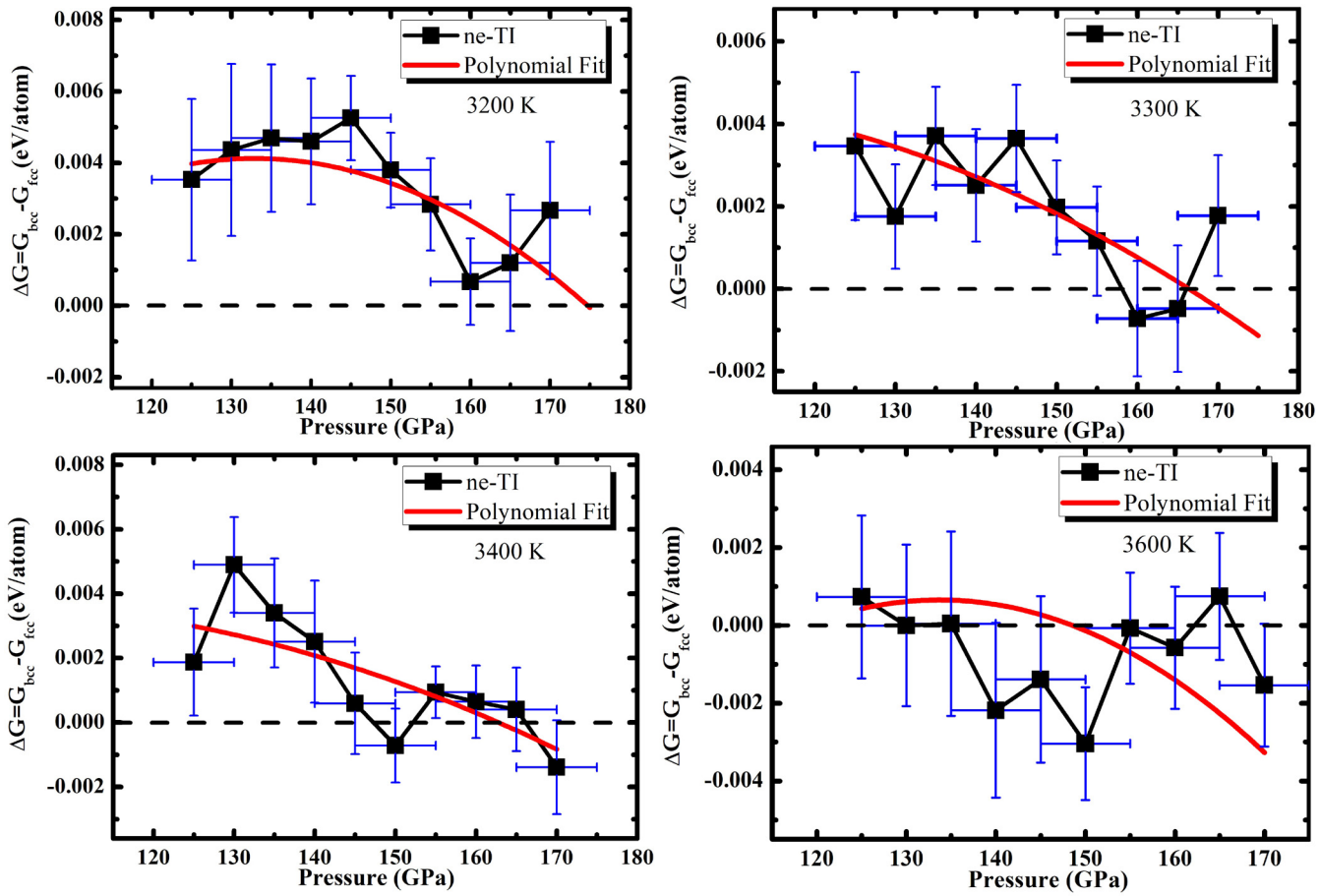

Figure S6. The free energy differences between FCC and shock-induced BCC under four temperatures. The free energy of FCC and shock-induced BCC have been calculated in large range of pressure, every data are averaged by three points. The curves were second-order polynomials. Dot line denotes the free energy differences equal to zero, corresponding to the phase transition.